The dynamics of FTO binding and demethylation from the m^{6}A motifs

Yixing Li[1#], Kejing Wu[2#], Weili Quan[2,3#], Lin Yu[1], Shuang Chen[3], Chao Cheng[2], Qijia Wu[3†], Shuhong Zhao[4], Yi Zhang[2,3*], Lei Zhou[1*]

[1]State Key Laboratory for Conservation and Utilization of Subtropical Agro-bioresources, College of Animal Science and Technology, Guangxi University, Nanning, P.R. China

[2]Center for Genome Analysis, ABLife Inc., Wuhan, Hubei 430075, China.

[3]Laboratory for Genome Regulation and Human Health, ABLife Inc., Wuhan, Hubei 430075, China.

[4]Key Lab of Agricultural Animal Genetics and Breeding, Ministry of Education, College of Animal Science and Veterinary Medicine, Huazhong Agricultural University, Wuhan, 430070, P. R. China.

[#]These authors contributed equally to this work and were joint first authors.

***Corresponding author:**

Yi Zhang: yizhang@ablife.cc; Tel: 86-13317198317; Fax: 86-27-8177-9056

Lei Zhou: zhoulei@gxu.edu.cn; Tel: 86-771-3231158

[†]Present address: Healthiness Technology Co., Ltd. Building C2, No.666 Xiaoping Road, Wuhan East Lake High-tech Development Zone, Wuhan 430074，China.

ABSTRACT

N^6-methyladenosine (m^{6}A) is considered as a reversible RNA modification occurring more frequently on the GAC than AAC context *in vivo*, which regulates post-transcriptional gene expression in mammalian cells. m^{6}A “writers” METTL3 and METTL14 demonstrate a strong preference for binding AC-containing motifs in living cells. However, this evidence is currently lacking for m^{6}A erasers, leaving the dynamics of the internal m^{6}A modification under debate recently. We analyzed three recently published FTO CLIP-seq data sets and two generated in this study, one of the two known m^{6}A “erasers”. FTO binding peaks from all cell lines contain RRACH motifs. Only those from K562, 3T3-L1and HeLa cells were enriched in AC-containing motifs, while those from HEK293 were not. The exogenously overexpressed FTO effectively binds to m^{6}A motif-containing RNA sites. FTO overexpression specifically removed m^{6}A modification from GGACU and RRACU motifs in a concentration-dependent manner. These findings underline the dynamics of FTO in target selection, which is predicted to contribute to both the m^{6}A dynamics and the FTO plasticity in biological functions and diseases.

KEYWORDS： FTO; m^{6}A; demethylases; RNA modification; CLIP-seq

Introduction

In early 1970s, several groups found that the methylation modification is not restricted to rRNAs and tRNAs, also occurs in polyadenylated cellular [1, 2] and viral [3-5] mRNAs. The methylated nucleosides in mRNAs were further determined as the 5'-terminal $m^7G(5')ppp(5')Nm$ [6-9] and the internal *N*^{6}-methyl adenosine (m^6A) [10-12]. The dimethylated nucleoside, *N*^{6}, 2'-*O*-dimethyladenosine (m^6Am), and the four common 2'-*O*-methylribonucleosides (Gm, Am, Um, Cm) at the second position were reported soon after [9]. Then, internal m^6A was reported to occur primarily in two sequence contexts, Gm^6AC (70%) and Am^6AC (30%) in HeLa cell [13], and 60% in Gm^6AC in SV40 mRNA [14].

Recently, MeRIP-Seq (methylated RNA immunoprecipitation followed by sequencing) technology, also called m^6A-seq, allows the mapping of m^6A sites at the whole-transcriptome level [15, 16]. MeRIP-seq and a miCLIP-seq (m^6A cross-linking) analysis confirmed that m^6A modification preferably occurs within the consensus motif RRACH (R = G or A; H = A, C, or U), more in the sequence context of GAC than AAC [15-17]. The currently published MeRIP-seq experiments commonly used a commercial antibody against both the internal m^6A and the 5'-terminal m^6Am [18-20]. miCLIP recovers mutation and truncations in cDNAs, which allows the mapping of about 18,000 high-confident cross-linking m^6A sites among which a few hundred associates with the 5' terminal m^6Am [17].

The RNA m^6A modification is considered a reversible modification in living cells. The reversible m^6A modification dictates the dynamics of m^6A modification in

62 transcriptomes, which has been shown to regulate multiple processes of RNA
63 metabolism, including alternative splicing, RNA stability and translation [21-27].
64 Consistently, m^{6}A modification modulates important biological processes, such as
65 stem cell differentiation, heat shock response, oocyte competence and early zygotic
66 development, neuronal and other development, and innate immunity [24, 26, 28-31], and is
67 also involved in cancers [32-38] and other diseases [39].

68 Nevertheless, a number of contradicting results have led to the current debate of
69 the m^{6}A dynamics [40-44]. m^{6}A is added by RNA methyltransferase (“writer’) and removed
70 by demethylases (“eraser”) [23, 45]. Photoactivatable ribonucleoside-enhanced
71 crosslinking and immunoprecipitation (PAR-CLIP) analysis has demonstrated that the
72 binding peaks of methyltransferase METTL3 and METTL14 are highly enriched in
73 RRACH motifs, consistent with a strong selection of the sequence context for their
74 writing of m^{6}A [46]. So far, two RNA demethylases, fat mass and obesity-associated
75 protein (FTO) and alkylated DNA repair protein AlkB homolog 5 (ALKBH5), have been
76 identified to remove m^{6}A modification [39, 47]. However, neither of them has been shown
77 to selectively bind to the internal m^{6}A motifs. *In vitro* studies showed that neither FTO
78 nor ALKBH5 shows strict dependence on RRACH motifs in their demethylation
79 activity[48], although the sequence and structure of RNAs affect the demethylation
80 activity of FTO [49]. Three recently published works have performed FTO CLIP-seq
81 experiments; however, none of them reports FTO binding of any m^{6}A motifs [50-52].
82 Moreover, a recent study showed that FTO could remove the methyl group from the
83 5’-cap m^{6}Am with a much higher efficiency than that from the internal m^{6}A [53]. Therefore,

it remains highly questionable whether FTO recognizes and removes m^{6}A from the internal m^{6}A motifs, which is a key of the m^{6}A reversibility and dynamics.

To investigate the FTO demethylation target sites in cells, we analyzed the published FTO CLIP data sets from human HEK293 cell line [50], mouse embryonic fibroblasts (3T3-L1) [51], and FTO eCLIP data set from human erythroleukemia K562 cell line [52]. FTO binding peaks from 3T3-L1 and K562 cells, but not from HEK293 cells, showed the presence of the GAC consensus in the top enriched motifs. We then performed FTO CLIP-seq in HeLa cells, showing that the GAC consensus was present in the top represented motifs. The m^{6}A motifs were more enriched in FTO binding peaks upon its overexpression. We further showed that overexpression of FTO robustly removed m^{6}A modification from RRACH motifs. Additionally, the number of transcripts subjected to FTO demethylation were increased with the FTO concentration. The cell type- and concentration-dependence of FTO binding and demethylation selectively from the internal m^{6}A motifs support the m^{6}A dynamics and reversibility.

Results

The m^{6}A context GAC is enriched in FTO binding peaks from K562 and 3T3-L1 but not in HEK293T

To study whether FTO selectively binds to RRACH motif, we firstly analyzed three FTO CLIP/eCLIP data sets which were generated by three different labs from HEK293 [50], K562 [52] and 3T3-L1 [51]. The usable reads could estimate library complexity indicative of the binding strength of a RNA binding protein [52]. FTO eCLIP-seq data contained significantly less usable reads than those of PTBP1 (K562), and much less in FTO

106 CLIP-seq data from HEK293 than that from K562 (Fig. S1a). This data profile could
107 indicate a weak RNA binding affinity of FTO with its targets.

108 Plot of the distribution of FTO eCLIP/CLIP-seq reads and peaks showed a
109 preferable location in the intronic region (Fig. S1b), consistent with its reported role in
110 regulating alternative splicing [24, 50]. When the regional distribution of CLIP/eCLIP reads
111 was normalized by pre-mRNA length in each genic region, FTO-bound reads were
112 enriched in 5'UTR in data sets from HEK293 and K562 (Fig. 1a). Consistent with the
113 reported high efficiency of FTO demethylation of the 5'-end m^6Am [53], a sharp
114 enrichment of FTO binding signals around the transcription start site (TSS) was clearly
115 demonstrated by all three replicates of CLIP-seq data from HEK293 cells, while the
116 FTO binding signals were depleted around the stop codon (Fig. 1b). However, the TSS
117 enrichment was not evident in the eCLIP-seq data from K562 cells, an enriched
118 distribution across the entire 5'UTR was instead observed. Meanwhile, the depleted
119 FTO binding at the stop codon and the 3' UTR region was seen, but to a much lesser
120 extent than that of HEK293 (Fig. 1b). The distribution profile of FTO CLIP reads from
121 3T3-L1 around the TSS was between HEK293 and K562 (Fig. 1b).

122 We next identified FTO binding peaks using three different pipelines, Piranha [54],
123 CIMS [55] and ABLIRC [56], all displaying similar peak distribution in different genomic
124 regions (Fig. S1c). A *de novo* motif search of the 5-mer motifs from ABLIRC peaks
125 using the HOMER algorithm revealed that the GAC- and/or GGAC-containing motifs
126 were overrepresented in FTO binding peaks from K562, particularly in 3T3-L1, but not
127 in those from HEK293T (Fig. 1c, and Fig. S2a). The search from CIMS peaks resulted

in the GGAC-containing overrepresented motif in one of K562 replicates, while no AC-containing motif was resulted from Piranha peaks from either K562 or HEK393 replicates (Fig. S2a). It should be noted that non-m^{6}A FTO-binding motifs were different among cell lines. For example, GA-rich motifs and UUURA motif were more overrepresented than GAC and GGAC-motifs in K562 cells in both replicates, and GUUCG motif was highly overrepresented in HEK293T cells in three replicates, based on the motif resulted from ABLIRC peaks (Fig. S2a).

Given that the percentage of usable reads for the HEK293T cells was low, we randomly extracted 102,470 usable reads from each of all samples to call FTO binding peaks and then perform motif analysis. The results showed the that GAC and GGAC-motifs were enriched in FTO peaks from K562 and 3T3-L1 cells, but not in those from HEK293T cells (Fig. 1c, lower and Fig. S2b). Therefore, FTO binding of both m^{6}A motifs and non-m^{6}A motifs showed cell type-dependence.

FTO binds to GAC-containing and RRACH motifs in HeLa cells, and the exogenously overexpressed FTO shows increased selectivity.

As suggested above, FTO might not strongly associate with the internal m^{6}A GAC motifs in some cell types. Theoretically, the increase of the cellular FTO concentrations would increase the concentration of FTO-target complex sensitive to CLIP-seq capture (Fig. 2a). To test this hypothesis, we overexpressed the Flag-tagged FTO excessively in HeLa cell line where the endogenous FTO expression level was low (Fig. S3a). Confocal fluorescence microscopy showed that FTO was localized both in nucleus and cytoplasm. When FTO was overexpressed, its localization in nucleus apparently

increased (Fig. S3b). The methylation level of total RNA and polyadenylated mRNA was then measured by dot blot analysis using antibody against both m^6A and m^6Am. It has been recently reported that the total amount of internal m^6A is at least 10-fold larger than the amount of 5'-end m^6Am in mRNAs, and FTO demethylates more m^6A than m^6Am in HeLa cells [49, 51]. FTO overexpression reduced the overall RNA methylation level as predicted, and a much more pronounced reduction was observed for total RNA than purified mRNA (Fig. S3c). This finding is in good agreement with the recent report that FTO has a higher preference to remove m^6A from the primary transcript level [57], and with the early findings of high m^6A occurrence in 18S and 28S rRNAs [1], as well as in tRNA [1, 19, 51].

Under this functional context of FTO overexpression, we performed CLIP-seq experiments similar to eCLIP to identify FTO binding targets. To exclude the potential artifacts associated with a specific antibody, we used anti-FTO antibody in normal HeLa cells for two biological replicates and anti-Flag antibody in FTO-overexpressing (FTO-Flag) and control (Flag control) HeLa cells. Please be noted that in the CLIP-seq library construction approach applied here, the 5' adapter was ligated to the 5'-end of RNase-digested RNA after the end repair. This should eliminate the ligation to the 5'-end m^6Am with a cap structure; only the FTO-bound m^6Am-containing RNA fragments without a 5' cap structure could be recovered together with the internal m^6A-containing RNA fragments. Both the FTO and Flag antibodies showed high specificity and efficiency in immunoprecipitation (Fig. S3d and S3e). The gel region containing protein–RNA complex above molecular weight of FTO and FTO-Flag was excised and

used for sequencing library preparation (Fig. S3f and Fig. S3g). A positive control CLIP library of PTBP1 was included. The data were summarized in Table S1.

We observed the similar low fraction of usable reads from FTO CLIP data in HeLa cells, while FTO overexpression increased the usable reads fraction (Fig. S4a). FTO CLIP tags in one replicate was highly accumulated near the FTO binding sites identified in the other biological replicate (Fig. S4b), demonstrating the confidence of the RNA binding activity of FTO. We further confirmed the specificity of the CLIP assay by performing UV-RIP-PCR analysis on a panel of anti-FTO enriched RNA fragments (Fig. S4d).

When compared with the enrichment in IgG controls, FTO CLIP reads did not enrich around the TSS nor 5'UTR region in normal HeLa cells (Fig. 2b, Fig. S4c). The overall FTO binding in transcribed regions were increased upon FTO overexpression (Fig. 2b, below). At the basal level of FTO expression, the majority of FTO binding peaks (46.43%-50.59%) were located in the intronic regions, similar as those of the previously published data (Fig. 2c, Fig S1c). When FTO was overexpressed in HeLa cells, the FTO binding peaks preferentially shifted to the protein coding regions (Fig. 2c).

Analysis of the 5-mer motifs showed that the most enriched motif harbored the GAC consensus sequence in both biological replicates of endogenous FTO binding sites (Fig. 2d and Fig. S4e). Upon FTO overexpression, motif enrichment scores increased consistent with the increased concentration of FTO-target RNA complex. Strikingly, the GAC-containing motif ranked as the most overrepresented one,

supporting that the exogenously expressed FTO was functional (Fig. 2d). When we increased the motif length during the motif search, the enrichment of GGAC and GGACU in top motifs appeared (Fig. S4f). We then calculated the fraction of FTO binding peaks containing GGACU motif and RRACH motifs in all the CLIP/eCLIP data. It is shown the peaks containing these m^{6}A motifs were presented in all cell lines, although the frequency differed. FTO overexpression increased the m^{6}A motif frequency in HeLa cells (Fig. 2e). Given that relative low percentage of usable reads for normal control (Fig. 4Sa), we randomly selected the same small number of usable reads as in Figure 1c (lower panel) from each sample to call FTO binding peaks and motif analysis. Similar results were obtained (Fig. S4g). These results confirmed that FTO binds to the m^{6}A sequence context, and suggested that the binding is sensitive to the FTO concentration.

FTO overexpression effectively removes m^{6}A modification from polyadenylated mRNA/lncRNAs at GGACU motifs in HeLa cells

Given that the overexpressed FTO-Flag bound to GGACU motif in HeLa cells, we then explored whether FTO-Flag could remove m^{6}A from this typical m^{6}A motifs, by performing m^{6}A-seq experiments to capture m^{6}A sites on polyadenylated mRNAs/lncRNAs in control (Flag-control) and FTO-overexpression (FTO-Flag) HeLa cells. The sequence data from two different benches of experiments was shown, with 22.2-fold (H) and 4.3-fold (L) of FTO overexpression by comparing the FPKM values of FTO in the corresponding input controls (Table S2, Fig.3a). Analysis of the input controls showed that the expression level of key m^{6}A writer and eraser genes was not

changed upon FTO overexpression, which eliminated the complication of the result interpretation (Fig. 3a).

Analysis of the distribution of all mapped reads revealed that 96.5%-99.7% of input and m^{6}A-seq reads of each sample were mapped to nuclear encoded protein genes, pseudogenes and long non-coding RNAs (Table S3), which supported the purity of mRNAs used in this study. For the following peak calling and motif analysis, only uniquely mapped reads were involved, which removed any remaining complication from tRNAs and rRNAs. We called m^{6}A peaks from m^{6}A-seq data by running ABLIRC pipeline and MACS, followed by a *de novo* motif search with the HOMER algorithm, using input reads as backgrounds. Motif analysis showed that in control cells (Flag-control), the most significantly enriched motifs in m^{6}A-bound peaks in both replicates were characterized by GGACU consensus sequence, which exactly matched the canonical m^{6}A motif (Fig. 3b). Consistent with the hypothesis that FTO demethylates from its bound m^{6}A motif, GGACU motif disappeared from the top-ranking motifs in FTO-overexpressed cells (Fig. 3b and Fig. S5a).

Calculating the ratio of RRACU-bearing peaks in all m^{6}A peaks confirmed the majority of peaks (52.90%~ 61.36%) detected in Flag-control cells contained RRACU motif, which reduced significantly (33.97%~36.91%) upon FTO overexpression (Fig. 3c). Additionally, the frequency of RRACU at the m^{6}A peak positions in FTO overexpressed cells was substantially lower than that observed at Flag-control cells (Fig. S5b). These results are all in line with the conclusion that FTO selectively erases

237 the m^{6}A modification from the RRACU motif of polyadenylated mRNAs/lncRNAs, likely
238 in a FTO concentration-sensitive manner.

239 To further study the FTO selectivity of RRACU motif for its “eraser” function, we
240 separated the m^{6}A peaks into two groups by either containing or lacking a RRACU
241 motif. We then plotted the m^{6}A-seq reads around the center of these m^{6}A peaks. In
242 accordance with the m^{6}A-demethylation activity of FTO, we observed a substantial
243 decreased amount of m^{6}A-seq reads around the center of peak containing RRACU
244 motif after FTO overexpression, in both sets of the experiments (Fig. 3d, upper and
245 Fig. S5c, left). In contrast, around the center of peaks lacking the RRACU consensus
246 sequence, the level of m^{6}A-seq reads was not decreased, but somewhat increased
247 upon FTO overexpression (Fig. 3d, upper and Fig. S5c, right)

248 As examples, FTO specifically removed m^{6}A signals from the RRACU-containing
249 peaks in 3’ UTRs of the apoptosis associated gene *DFFA* [58] and lipid metabolism genes
250 *PPARD* and *VLDLR* [59, 60] (Fig. 3e and Fig. S6), which contained the GGACU motif. It
251 is possible that FTO regulates body mass index and obesity, partially by specifically
252 removing the m^{6}A modification from *PPARD* and *VLDLR*. We also showed examples
253 whose m^{6}A levels were not decreased by FTO, and these m^{6}A modification occurred
254 at RRACU-lacking peaks. These included m^{6}A clusters on the internal exons of the
255 splicing factor *SFPQ* (Fig. 3e) and *RPL23A* (Fig. S6) and one cluster in the intronic
256 region of *ZNF701* (Fig. S6).

257 We further validated the dependence of RRACU motif for FTO demethylation by
258 RIP-qRT-PCR. Consistent with our findings above, all but one RRACU-bearing m^{6}A

sites showed decreased m^{6}A signals upon FTO overexpression, whereas all of those lacking RRACU motif showed unchanged or increased m^{6}A levels upon FTO overexpression (Fig. 3f). Taken together, overexpressed FTO preferentially removed m^{6}A modification from the GGACU motif.

The extent of FTO demethylation from mRNAs/lncRNAs is concentration-dependent

FTO selection of RRACH motif for m^{6}A demethylation in HeLa cells might represent a unique mechanism for FTO specificity in demethylating a population of genes but not the other. We noticed the m^{6}A peak calling approach was not sensitive to the genes with high mRNA level. For example, we found that FTO specifically removed m^{6}A modification from activating transcription factor ATF4 mRNA (Fig. 4a), a recently reported FTO target [61]. One m^{6}A modification being removed was well correlated with the reported alternative translation site controlled by m^{6}A dynamics (Fig. 4a). However, these m^{6}A modifications were not recovered by peak calling pipelines, due to the high input signals.

We therefore subjected m^{6}A-seq reads to the edgeR software to identify differentially methylated genes (DMG) associated with FTO overexpression. For both benches of overexpression experiments, a much larger number of DMGs were down-methylated compared with those up-methylated. We showed the down-methylated genes were 5,872 and 2030 and the up-methylated genes were 1679 and 893, for the 22.2-fold and 4.3-fold FTO overexpression, respectively (Fig. 4b). As control, the difference between the corresponding input samples was very small (Fig. 4b). The

281 extent of FTO demethylation of mRNA/lncRNAs was apparently concentration-
282 dependent (Fig. 3c and Fig. S5b).

283 We further showed that m^{6}A peak-containing genes from the control Flag samples
284 were more significantly overlapped with the FTO down-demethylated genes, than
285 those from samples with FTO overexpression (Fig. 4c). This further supported that the
286 FTO demethylation occurs at the m^{6}A-modified transcripts.

287 **Discussion**

288 The presented results together support a model for the dynamics of FTO in mediating
289 m^{6}A demethylation. FTO binds to GAC-containing and RRACH motifs in
290 mRNAs/lncRNAs typical for m^{6}A modification in a cell type-dependent manner. FTO
291 binds to m^{6}A motifs and removes the m^{6}A modification in a concentration-dependent
292 manner in HeLa cells. This model supports the m^{6}A dynamics and diverse regulatory
293 functions, and provides mechanistic insights into the FTO plasticity in biological
294 functions and its reported involvement in multiple diseases.

295 This is the first report showing that FTO recognizes and binds to m^{6}A motifs in cells,
296 which is similar to the two m^{6}A "writers" methyltransferases METTL3 and METTL14 [46].
297 Therefore, in contrast to non-selectively of the demethylation activity of two 'eraser'
298 proteins FTO and ALKBH5 *in vitro* [48], our results demonstrated that the selectively of
299 FTO binding and demethylation from m^{6}A motifs in living cells. In fact, a recent *in vitro*
300 studies showed both the tertiary structure and sequence of the RNA substrates can
301 affect the catalytic activity of FTO [49]. Our results are consistent with the recent findings

of the specific targets of FTO and ALKBH5 involved in diverse biological functions [35, 37, 61-63].

We have showed that FTO binds mRNA/lncRNA towards GAC-containing and RRACH motifs in multiple cell lines, with its motif selectivity being cell-type dependent. The association between FTO and m^{6}A motifs is enhanced by FTO overexpression, and the overexpressed FTO preferentially removes m^{6}A modification from GGACU and RRACU motifs also in a concentration-dependent manner, at least in HeLa cells. We propose that the concentration-dependence of FTO action shall contribute to the observed m^{6}A/m^{6}Am dynamics and enable a larger regulatory plasticity of m^{6}A/m^{6}Am mark under different physiological and pathological states. Given the structural and functional similarity between FTO and ALKBH5, it could be possible that ALKBH5 also contacts with the internal m^{6}A similarly.

The finding of FTO binding and demethylation from the internal m^{6}A motifs might reconciliate some of the recent conflicted results. For example, Mauer *et al*. showed that FTO controls mRNA stability in HEK293T cells with its demethylation activity towards m^{6}Am [53]. Results from the other two groups showed certain contradiction [51, 64], which add the debate in this field. In one study, FTO demethylation on internal m^{6}A has a greater effect on mRNA stability than the ones with cap m^{6}Am in the tested cells [51]. In the other study, m^{6}Am promotes the translation of capped mRNAs, but not stabilize A-starting capped mRNAs [64].In the context of the findings presented in this study, the discrepancy might be resulted from the different FTO expression levels and cell lines among these studies. In fact, one of these two studies demonstrates that the

efficiency of FTO in demethylating m^{6}A and m^{6}Am is distinct among different cell lines, which depends on the relative levels of m^{6}A/m^{6}Am and the nucleus and cytoplasm distribution of FTO protein [51].

Additionally, our analysis showed that FTO binding was mostly enriched at the TSS region in HEK293 cells, although the CLIP-seq method applied to obtain the data disfavor the recovery of FTO-bound m^{6}Am-containing RNA fragments with an intact 5' cap [50]. This finding is well correlated with the previously reported high preference of FTO for m^{6}Am as a substrate [53], if we assume that at least a fraction of the TSS binding signals of FTO represents its demethylation of m^{6}Am. The more preferred distribution of FTO binding sites in the 5'UTR and 3'UTR body regions of K562 and HeLa cells is consistent with the reported functions and the m^{6}A profiles regulated by FTO in other leukemia cells and mouse embryonic fibroblasts [34, 37]. We suggest that the cell type-dependent binding of FTO, a potential indicator of its demethylation target selection, should be taken into account in explaining data in the future studies.

In conclusion, we have demonstrated the selectivity of FTO in binding and erasing m^{6}A modification from m^{6}A motifs, which support FTO functions in regulating the dynamics and distribution of m^{6}A/m^{6}Am mark under different physiological and pathological states [26, 34, 37, 50, 51, 65-68]. We propose that FTO-mRNA/lncRNA association is weak, which leaves rooms for additional cellular factors to corporately work with this eraser to choose among the internal m^{6}A sites and 5'-end m^{6}Am in different transcripts. The dynamics of FTO in target selection is predicted to be sensitive to physiological and pathological changes, and contribute to both m^{6}A dynamics and the FTO plasticity

in biological functions and its reported involvement in multiple diseases. Further study of the FTO dynamics and m^6A/m^6Am demethylation regulation should be critical for m^6A biology and the related disease control.

Materials and methods

Cell culture, Plasmid and transfection

HeLa cells were cultured in Dulbecco's Modified Eagle Medium (DMEM) (Gibco) supplemented with 10% fetal bovine serum (FBS) (Hyclone) and 1% penicillin/streptomycin (Hyclone) at 37 ℃ in a humidified incubator with 5% CO2.

The cDNA of human FTO gene (GenBank: NM_001080432.2) amplified by PCR and subcloned into pCMV-Tag.2B-Flag vector (Stratagene). pCMV-Tag.2B-Flag vector containing FTO gene (FTO-Flag) or not containing FTO gene (Flag-control) were transfected into HeLa cells using Lipofectamine 2000 (Invitrogen, 11668-027) following manufacturer's instructions.

Western blots

Total protein lysate was extracted from FTO overexpression/control cells with RIPA buffer. 40-60 μg protein extracts were separated by SDS-PAGE and transferred to PVDF membranes (Bio-Rad, cat. 1620177, Foster, California, USA). Membranes were blocked with 5% non-fat milk, followed by overnight incubation with primary antibodies against either FTO (CUSABIO, Shanghai) or Flag (Sigma, cat. F7425) overnight at R.T. After the incubation with Rhodamine (TRTTC) goat anti-rabbit IgG (Abclonal, cat.

A5040) (1: 10,000) for 1 hour at R.T, the signals were detected with Clarity Max™ Western ECL Substrate (Bio-Rad, cat. 1705062).

Immunofluorescence analysis

After washed with PBS, HeLa was fixed in 4% formaldehyde. Cells were blocked in 5% BSA in PBS with 0.2% Triton X-100 for 10 min. Cells were incubated with antibody against FTO (MBL, RN121PW) overnight at 4 °C. After washing with PBS, cells were incubated with an anti-rabbit IgG (Abclonal, cat. A5040) (1:100) in the dark at R.T for 1 hour. DAPI staining for DNA was performed. Images were obtained using a confocal LSM780 microscope (Carl Zeiss, Germany).

CLIP-seq

HeLa cells (~10^6) cultured to a confluence of 70-80% with or without FTO-Flag or Flag transfection were subjected to UV cross-linking treatment on ice for 400 mJ/cm2. The cross-linked cells were then lysed and treated with RQ1 RNase-Free DNase (Progema, cat. M6101) to prevent DNA contamination, followed by partially digestion with MNase (Thermo, cat. EN0181) to further release the FTO-protected RNA fragments in a FTO-RNA complex form. FTO–RNA complex was immunoprecipitated by incubating with DynaBeads protein A/G conjugated with anti-FTO antibody (MBL, cat. RN121PW, Japan), IgG (Millipore, cat. 12-370, USA) or anti-Flag antibody (sigma, cat. F7425, USA) at 4 °C for 2 hours. Efficiency of the immunoprecipitation of was showed in Fig. S3. RNA was dephosphorylated at 3’ end and phosphorylated at 5’ end. The protein–RNA complex was separated by 4-12% NuPAGE Bis-Tris gel (Nvirogen, cat. NP0321 BOX) and the region of the membrane 30 kDa above the protein size was excised (Fig.

S3e). Protein was digested by proteinase K and RNA was isolated to prepare sequencing library using Balancer sm/miRNA Library Preparation Kit according to the manufacturer's instructions (Gnomegen, cat. K02420). The cDNA libraries were subsequently quantified and sequenced on the Illumina Nextseq platform. Image processing and base-calling were performed by Illumina pipeline.

Analysis of CLIP-seq data

The clean reads were generated from raw sequencing reads after removing adaptor sequences and low quality sequences, which were mapped to human GRCh38 genome using Tophat (v2.1.1). Reads aligned to more than one genome location were discarded. 'Usable' reads were defined as reads that uniquely mapped to the genome and remained after discarding PCR duplicates.

FTO CLIP-seq peaks were identified by running Piranha,[54] CIMS[55] and ABLIRC.[56] The target genes of FTO were finally determined by analyzing the genomic locations of all the FTO binding peaks. A *de novo* motif search with the HOMER algorithm[69] was performed to identify FTO binding sites.

UV-RIP-qPCR

HeLa cells (~10^6) were UV cross-linked, which were operated similarly as CLIP-seq described above to obtain the cross-linked protein-RNA complex right after immunoprecipitation, without further treatment. MNase was not used to further fragment RNA associated with FTO. Then, RNA was purified from the protein-RNA complex by proteinase K treatment, phenol/chloroform extraction and precipitated with ethanol. The isolated FTO-associated RNA was reverse transcribed using random

primer, and analyzed by quantitative, strand-specific RT-PCR using the Real-time detection system using a QuantStudio 6 Flex System (ABI). Gene-specific PCR primer pairs were presented in Table S4.

m^{6}A dot blot assay

Total RNA was extracted using TRIzol Reagent (Ambion) following the manufacturer's instructions, and mRNA were then purified by GenElute™ mRNA Miniprep Kit (sigma, MRN10). The m^{6}A-dot-blot was performed on the Bio-Dot®Microfiltration Apparatus (170-6545, GE Healthcare) using Amersham Hybond-N+ membrane (GE Amersham, RPN303B) in two-fold dilutions. After UV crosslinking, the blotted membrane was washed by 1×PBST buffer, blocked with 5% of non-fat milk, and incubated with primary rabbit anti-m^{6}A antibody (sysy, cat. 202003) overnight at 4 °C. After incubated with Horseradish peroxidase (HRP)-conjugated anti-rabbit IgG (DakoCytomation, p0448) secondary antibody, the membrane was visualized by supersignal westPico ECL substrate box (Thermo Pierce, 34087).

m^{6}A immunoprecipitation and m^{6}A-seq

The polyadenylated mRNAs isolated from total RNA using GenElute™ mRNA Miniprep Kit (sigma, MRN10) were fragmented into 100 nt length by using RNA Fragmentation buffer (0.1M Tris-HCL PH 7.0, 0.1M $ZnCl_2$). Then, 50 and 100 ng fragmented mRNAs were incubated for 2 hours at 4 °C with 12.5 μg of anti-m^{6}A antibody (sysy, 202003) in IP buffer (0.05M Tris-HCL pH 7.4, 0.375M NaCl, 0.5% Igepal CA-630). The mixture was then subjected to immunoprecipitation by incubation with Pierce™ ChIP-grade Protein A/G Magnetic Beads (Thermo, 26162) at 4 °C for 2 hours. After sufficient

washing, m^{6}A antibody-bound RNA was eluted from the beads with Elution buffer (1×IP buffer, 7mM m^{6}A, RNase inhibitor), and then ethanol-precipitated. The eluted RNA was resuspended in H_2O and used to generate the cDNA library according to RNA-Seq Library Preparation Kit for Transcriptome Discovery–Illumina Compatible, which was then sequenced using the HiSeq 2000 system (Illumina) according to the manufacturer's instructions.

Analysis of m^{6}A_seq data

For m^{6}A-Seq data, adaptors and low quality bases were trimmed from raw sequencing reads using CutAdapt, and reads less than 16nt were discarded. After quality control and data filtering, reads were aligned to the reference genome GRCh38 by TopHat2 (v2.1.1). To assess m^{6}A level of each gene, only reads unambiguously aligned were preserved to calculate reads number and RPKM value (RPKM represents reads per kilobase and per million). To identify the m^{6}A regions (statistically significant m^{6}A peaks), we called m^{6}A peaks from m^{6}A-seq data by running ABLIRC pipeline [56].

m^{6}A-qRT-PCR

m^{6}A immunoprecipitation was performed as above. The ethanol-precipitated m^{6}A antibody-bound RNA fragments were reverse transcribed using random primer, and then subjected to quantitative, strand-specific RT-PCR sing the Real-time detection system using a QuantStudio 6 Flex System (ABI). Gene-specific PCR primer pairs were presented in Table S5.

Differentially demethylated genes (DMG)

Differentially demethylated genes between the paired groups were analyzed by using edgeR in R packages4. For each gene, significance p-value was obtained based on the model of negative binomial distribution. Fold changes of gene expression were also estimated within the edgeR statistical package. The criterion for DMG has been set as fold change >2 or <0.5 and $P < 0.01$.

Statistical analysis

For the comparison of proportions of m^6A peaks with or without the RRACU motif and the qPCR results, statistical analyses were carried out using Student' s t-test. The results of qPCR are shown as the mean ± SE. Statistical analysis was performed using R (v3.1.3).

Data availability

All CLIP-seq and m^6A-seq data from this study have been submitted to the NCBI Gene Expression Omnibus (GEO; http://www.ncbi.nlm.nih.gov/geo/) under accession number GSE101955. PTB CLIP data are available at NCBI with BioProject ID: PRJNA377229 (https://www.ncbi.nlm.nih.gov/bioproject/?term=PRJNA377229). A link to a UCSC genome browser session displaying the uploaded sequence tracks has been created (https://genome.ucsc.edu/cgi-bin/hgTracks?hgS_doOtherUser=submit&hgS_otherUserName=erhuoyi&hgS_otherUserSessionName=fto).

Acknowledgements

We are grateful to Yaqiang Xue, and Yali Ye (ABLife) for their contributions to the experimental parts, and to Yaxun Wei (ABLife) in helping some graphics. This work

476 was supported by the grants from National Key R&D Program of China
477 (2018YFD0500402), National Natural Science Foundation of China (31660641),
478 Guangxi Natural Science Foundation (2017GXNSFAA198139), Guangxi Hundred-
479 Talent Program, State Key Laboratory for Conservation and Utilization of Subtropical
480 Agro-bioresources (SKLCUSA-a201808), and Scientific Research Foundation of
481 Guangxi University (XTZ130719). This study is also supported by grant from ABLife
482 Inc. (ABL2013-07002).

483 **Disclosure of Interest**

484 No potential conflict of interest was reported by the authors.

485

REFERENCES

1. Desrosiers R, Friderici K, Rottman F. Identification of methylated nucleosides in messenger RNA from Novikoff hepatoma cells. Proc Natl Acad Sci U S A 1974; 71:3971-5.

2. Perry RP, Kelley DE. Existence of methylated messenger RNA in mouse L cells. Cell 1974; 1:37-42.

3. Furuichi Y. “Methylation-coupled” transcription by virus-associated transcriptase of cytoplasmic polyhedrosis virus containing double-stranded RNA. Nucleic Acids Res 1974; 1:809-22.

4. Rhodes DP, Moyer SA, Banerjee AK. In vitro synthesis of methylated messenger RNA by the virion-associated RNA polymerase of vesicular stomatitis virus. Cell 1974; 3:327-33.

5. Shatkin AJ. Methylated messenger RNA synthesis *in vitro* by purified reovirus. Proc Natl Acad Sci U S A 1974; 71:3204-7.

6. Abraham G, Rhodes DP, Banerjee AK. The 5' terminal structure of the methylated mRNA synthesized in vitro by vesicular stomatitis virus. Cell 1975; 5:51-8.

7. Furuichi Y, Miura K-I. A blocked structure at the 5' terminus of mRNA from cytoplasmic polyhedrosis virus. Nature 1975; 253:374.

8. Furuichi Y, Morgan M, Muthukrishnan S, Shatkin AJ. Reovirus messenger RNA contains a methylated, blocked 5'-terminal structure: m-7G(5')ppp(5')G-MpCp. Proc Natl Acad Sci U S A 1975; 72:362-6.

9. Wei CM, Gershowitz A, Moss B. 5'-Terminal and internal methylated nucleotide

508 sequences in HeLa cell mRNA. Biochemistry 1976; 15:397-401.
509 10. Adams JM, Cory S. Modified nucleosides and bizarre 5'-termini in mouse myeloma
510 mRNA. Nature 1975; 255:28-33.
511 11. Furuichi Y, Morgan M, Shatkin AJ, Jelinek W, Salditt-Georgieff M, Darnell JE.
512 Methylated, blocked 5 termini in HeLa cell mRNA. Proc Natl Acad Sci U S A 1975;
513 72:1904-8.
514 12. Wei C, Gershowitz A, Moss B. N^6, $O^{2'}$-dimethyladenosine a novel methylated
515 ribonucleoside next to the 5' terminal of animal cell and virus mRNAs. Nature 1975;
516 257:251-3.
517 13. Wei CM, Moss B. Nucleotide sequences at the N^6-methyladenosine sites of HeLa
518 cell messenger ribonucleic acid. Biochemistry 1977; 16:1672-6.
519 14. Canaani D, Kahana C, Lavi S, Groner Y. Identification and mapping of N^6-
520 methyladenosine containing sequences in simian virus 40 RNA. Nucleic Acids Res
521 1979; 6:2879-99.
522 15. Meyer KD, Saletore Y, Zumbo P, Elemento O, Mason CE, Jaffrey SR.
523 Comprehensive analysis of mRNA methylation reveals enrichment in 3' UTRs and near
524 stop codons. Cell 2012; 149:1635-46.
525 16. Dominissini D, Moshitch-Moshkovitz S, Schwartz S, Salmon-Divon M, Ungar L,
526 Osenberg S, et al. Topology of the human and mouse m^6A RNA methylomes revealed
527 by m^6A-seq. Nature 2012; 485:201-6.
528 17. Linder B, Grozhik AV, Olarerin-George AO, Meydan C, Mason CE, Jaffrey SR.
529 Single-nucleotide-resolution mapping of m6A and m6Am throughout the transcriptome.

530 Nat Methods 2015; 12:767-72.

531 18. Jia G, Fu Y, Zhao X, Dai Q, Zheng G, Yang Y, et al. N6-methyladenosine in nuclear

532 RNA is a major substrate of the obesity-associated FTO. Nat Chem Biol 2011; 7:885-

533 7.

534 19. Munns TW, Liszewski MK, Sims HF. Characterization of antibodies specific for N6-

535 methyladenosine and for 7-methylguanosine. Biochemistry 1977; 16:2163-8.

536 20. Bringmann P, Luhrmann R. Antibodies specific for N^6-methyladenosine react with

537 intact snRNPs U2 and U4/U6. FEBS Lett 1987; 213:309-15.

538 21. Fu Y, Jia G, Pang X, Wang RN, Wang X, Li CJ, et al. FTO-mediated formation of

539 N^6-hydroxymethyladenosine and N^6-formyladenosine in mammalian RNA. Nat

540 commun 2013; 4:1798.

541 22. Wang X, Lu Z, Gomez A, Hon GC, Yue Y, Han D, et al. N^6-methyladenosine-

542 dependent regulation of messenger RNA stability. Nature 2013; 505:117-20.

543 23. Meyer KD, Jaffrey SR. The dynamic epitranscriptome: N^6-methyladenosine and

544 gene expression control. Nat Rev Mol Cell Biol 2014; 15:313-26.

545 24. Zhao X, Yang Y, Sun BF, Shi Y, Yang X, Xiao W, et al. FTO-dependent

546 demethylation of N6-methyladenosine regulates mRNA splicing and is required for

547 adipogenesis. Cell Res 2014; 24:1403-19.

548 25. Meyer Kate D, Patil Deepak P, Zhou J, Zinoviev A, Skabkin Maxim A, Elemento O,

549 et al. 5′ UTR m^6A promotes cap-independent translation. Cell 2015; 163:999-1010.

550 26. Zhou J, Wan J, Gao X, Zhang X, Jaffrey SR, Qian SB. Dynamic m^6A mRNA

551 methylation directs translational control of heat shock response. Nature 2015;

526:591-4.

27. Yang Y, Fan X, Mao M, Song X, Wu P, Zhang Y, et al. Extensive translation of circular RNAs driven by N^6-methyladenosine. Cell Res 2017; 27:626-41.

28. Zheng Q, Hou J, Zhou Y, Li Z, Cao X. The RNA helicase DDX46 inhibits innate immunity by entrapping m^6A-demethylated antiviral transcripts in the nucleus. Nat Immunol 2017; 18:1094-103.

29. Chen T, Hao YJ, Zhang Y, Li MM, Wang M, Han W, et al. m^6A RNA methylation is regulated by microRNAs and promotes reprogramming to pluripotency. Cell Stem Cell 2015; 16:289-301.

30. Haussmann IU, Bodi Z, Sanchez-Moran E, Mongan NP, Archer N, Fray RG, et al. m^6A potentiates Sxl alternative pre-mRNA splicing for robust Drosophila sex determination. Nature 2016; 540:301-4.

31. Ivanova I, Much C, Di Giacomo M, Azzi C, Morgan M, Moreira PN, et al. The RNA m^6A reader YTHDF2 is essential for the post-transcriptional regulation of the maternal transcriptome and oocyte competence. Mol Cell 2017; 67:1-9.

32. Liu J, Eckert MA, Harada BT, Liu S-M, Lu Z, Yu K, et al. m^6A mRNA methylation regulates AKT activity to promote the proliferation and tumorigenicity of endometrial cancer. Nat Cell Biol 2018; 20:1074-83.

33. Chen M, Wei L, Law CT, Tsang FH, Shen J, Cheng CL, et al. RNA N6-methyladenosine methyltransferase-like 3 promotes liver cancer progression through YTHDF2-dependent posttranscriptional silencing of SOCS2. Hepatology 2018; 67:2254-70.

574 34. Li Z, Weng H, Su R, Weng X, Zuo Z, Li C, et al. FTO plays an oncogenic role in
575 acute myeloid leukemia as a N^6-methyladenosine RNA demethylase. Cancer Cell 2017;
576 31:127-41.
577 35. Cui Q, Shi H, Ye P, Li L, Qu Q, Sun G, et al. m^6A RNA methylation regulates the
578 self-renewal and tumorigenesis of glioblastoma stem cells. Cell Rep 2017; 18:2622-
579 34.
580 36. Barbieri I, Tzelepis K, Pandolfini L, Shi J, Millan-Zambrano G, Robson SC, et al.
581 Promoter-bound METTL3 maintains myeloid leukaemia by m^6A-dependent translation
582 control. Nature 2017; 552:126-31.
583 37. Su R, Dong L, Li C, Nachtergaele S, Wunderlich M, Qing Y, et al. R-2HG exhibits
584 anti-tumor activity by targeting FTO/m^6A/MYC/CEBPA signaling. Cell 2018; 172:1-16.
585 38. Zhang C, Samanta D, Lu H, Bullen JW, Zhang H, Chen I, et al. Hypoxia induces
586 the breast cancer stem cell phenotype by HIF-dependent and ALKBH5-mediated m^6A-
587 demethylation of NANOG mRNA. Proc Natl Acad Sci U S A 2016; 113:E2047-E56.
588 39. Zheng G, Dahl JA, Niu Y, Fedorcsak P, Huang C-M, Li Charles J, et al. ALKBH5 is
589 a mammalian RNA demethylase that impacts RNA metabolism and mouse fertility. Mol
590 Cell 2013; 49:18-29.
591 40. Zhao BS, Nachtergaele S, Roundtree IA, He C. Our views of dynamic N^6-
592 methyladenosine RNA methylation. RNA 2018; 24:268-72.
593 41. Mauer J, Jaffrey SR. FTO, m^6Am, and the hypothesis of reversible
594 epitranscriptomic mRNA modifications. FEBS Lett 2018; 592:2012-22.
595 42. Darnell RB, Ke S, Darnell JE. Pre-mRNA processing includes N^6 methylation of

596 adenosine residues that are retained in mRNA exons and the fallacy of “RNA
597 epigenetics”. RNA 2018; 24:262-7.
598 43. Rosa-Mercado NA, Withers JB, Steitz JA. Settling the m^{6}A debate: methylation of
599 mature mRNA is not dynamic but accelerates turnover. Genes Dev 2017; 31:957-8.
600 44. Meyer KD, Jaffrey SR. Rethinking m^{6}A readers, writers, and erasers. Annu Rev
601 Cell Dev Biol 2017; 33:319-42.
602 45. Fu Y, Dominissini D, Rechavi G, He C. Gene expression regulation mediated
603 through reversible m^{6}A RNA methylation. Nat Rev Genet 2014; 15:293-306.
604 46. Liu J, Yue Y, Han D, Wang X, Fu Y, Zhang L, et al. A METTL3-METTL14 complex
605 mediates mammalian nuclear RNA N^6-adenosine methylation. Nat Chem Biol 2014;
606 10:93-5.
607 47. Huang Y, Yan J, Li Q, Li J, Gong S, Zhou H, et al. Meclofenamic acid selectively
608 inhibits FTO demethylation of m^{6}A over ALKBH5. Nucleic Acids Res 2015; 43:373-84.
609 48. Zou S, Toh JD, Wong KH, Gao YG, Hong W, Woon EC. N^6-Methyladenosine: a
610 conformational marker that regulates the substrate specificity of human demethylases
611 FTO and ALKBH5. Sci Rep 2016; 6:25677.
612 49. Zhang X, Wei LH, Wang Y, Xiao Y, Liu J, Zhang W, et al. Structural insights into
613 FTO's catalytic mechanism for the demethylation of multiple RNA substrates. Proc Natl
614 Acad Sci U S A 2019; 116:2919-24.
615 50. Bartosovic M, Molares HC, Gregorova P, Hrossova D, Kudla G, Vanacova S. N6-
616 methyladenosine demethylase FTO targets pre-mRNAs and regulates alternative
617 splicing and 3'-end processing. Nucleic Acids Res 2017; 45:11356-70.

618 51. Wei J, Liu F, Lu Z, Fei Q, Ai Y, He PC, et al. Differential m^6A, m^6Am, and m^1A
619 demethylation mediated by FTO in the cell nucleus and cytoplasm. Mol Cell 2018;
620 71:973-85.
621 52. Van Nostrand EL, Pratt GA, Shishkin AA, Gelboin-Burkhart C, Fang MY,
622 Sundararaman B, et al. Robust transcriptome-wide discovery of RNA-binding protein
623 binding sites with enhanced CLIP (eCLIP). Nat Methods 2016; 13:508-14.
624 53. Mauer J, Luo X, Blanjoie A, Jiao X, Grozhik AV, Patil DP, et al. Reversible
625 methylation of m^6Am in the 5' cap controls mRNA stability. Nature 2017; 541:371-5.
626 54. Uren PJ, Bahrami-Samani E, Burns SC, Qiao M, Karginov FV, Hodges E, et al.
627 Site identification in high-throughput RNA-protein interaction data. Bioinformatics 2012;
628 28:3013-20.
629 55. Moore MJ, Zhang C, Gantman EC, Mele A, Darnell JC, Darnell RB. Mapping
630 Argonaute and conventional RNA-binding protein interactions with RNA at single-
631 nucleotide resolution using HITS-CLIP and CIMS analysis. Nat Protoc 2014; 9:263-93.
632 56. Xia H, Chen D, Wu Q, Wu G, Zhou Y, Zhang Y, et al. CELF1 preferentially binds
633 to exon-intron boundary and regulates alternative splicing in HeLa cells. Biochim
634 Biophys Acta 2017; 1860:911-21.
635 57. Ke S, Pandya-Jones A, Saito Y, Fak JJ, Vagbo CB, Geula S, et al. m^6A mRNA
636 modifications are deposited in nascent pre-mRNA and are not required for splicing but
637 do specify cytoplasmic turnover. Genes Dev 2017; 31:990-1006.
638 58. Liu X, Zou H, Slaughter C, Wang X. DFF, a heterodimeric protein that functions
639 downstream of caspase-3 to trigger DNA fragmentation during apoptosis. Cell 1997;

640 89:175-84.

641 59. Seedorf U, Aberle J. Emerging roles of PPARδ in metabolism. Biochim Biophys

642 Acta 2007; 1771:1125-31.

643 60. Tacken PJ, Hofker MH, Havekes LM, van Dijk KW. Living up to a name: the role

644 of the VLDL receptor in lipid metabolism. Curr Opin Lipidol 2001; 12:275-9.

645 61. Zhou J, Wan J, Shu XE, Mao Y, Liu X-M, Yuan X, et al. N^6-methyladenosine guides

646 mRNA alternative translation during integrated stress response. Mol Cell 2018; 69:1-

647 12.

648 62. Zhang S, Zhao BS, Zhou A, Lin K, Zheng S, Lu Z, et al. m^6A demethylase ALKBH5

649 maintains tumorigenicity of glioblastoma stem-like cells by sustaining FOXM1

650 expression and cell proliferation program. Cancer Cell 2017; 31:591-606.

651 63. Zhang S-Y, Zhang S-W, Liu L, Meng J, Huang Y. m^6A-driver: identifying context-

652 specific mRNA m^6A methylation-driven gene interaction networks. PLoS Comp Biol

653 2016; 12:e1005287.

654 64. Akichika S, Hirano S, Shichino Y, Suzuki T, Nishimasu H, Ishitani R, et al. Cap-

655 specific terminal N^6-methylation of RNA by an RNA polymerase II–associated

656 methyltransferase. Science 2018:eaav0080.

657 65. Shun Z, Zhou‐Lan B, Di X, Zhi‐Jun Z, Ren Z, Yan‐Yang W, et al. FTO

658 regulates the chemo‐radiotherapy resistance of cervical squamous cell carcinoma

659 (CSCC) by targeting β-catenin through mRNA demethylation. Mol Carcinog 2018;

660 57:590-7.

661 66. Mathiyalagan P, Adamiak M, Mayourian J, Sassi Y, Liang Y, Agarwal N, et al. FTO-

662 dependent m6A regulates cardiac function during remodeling and repair. Circulation
663 2018.
664 67. Engel M, Eggert C, Kaplick PM, Eder M, Röh S, Tietze L, et al. The role of m^6A/m-
665 RNA methylation in stress response regulation. Neuron 2018; 99:389-403.
666 68. Xiang Y, Laurent B, Hsu CH, Nachtergaele S, Lu Z, Sheng W, et al. RNA m^6A
667 methylation regulates the ultraviolet-induced DNA damage response. Nature 2017;
668 543:573-6.
669 69. Heinz S, Benner C, Spann N, Bertolino E, Lin YC, Laslo P, et al. Simple
670 Combinations of Lineage-Determining Transcription Factors Prime cis-Regulatory
671 Elements Required for Macrophage and B Cell Identities. Mol Cell 2010; 38:576-89.
672
673

Figures

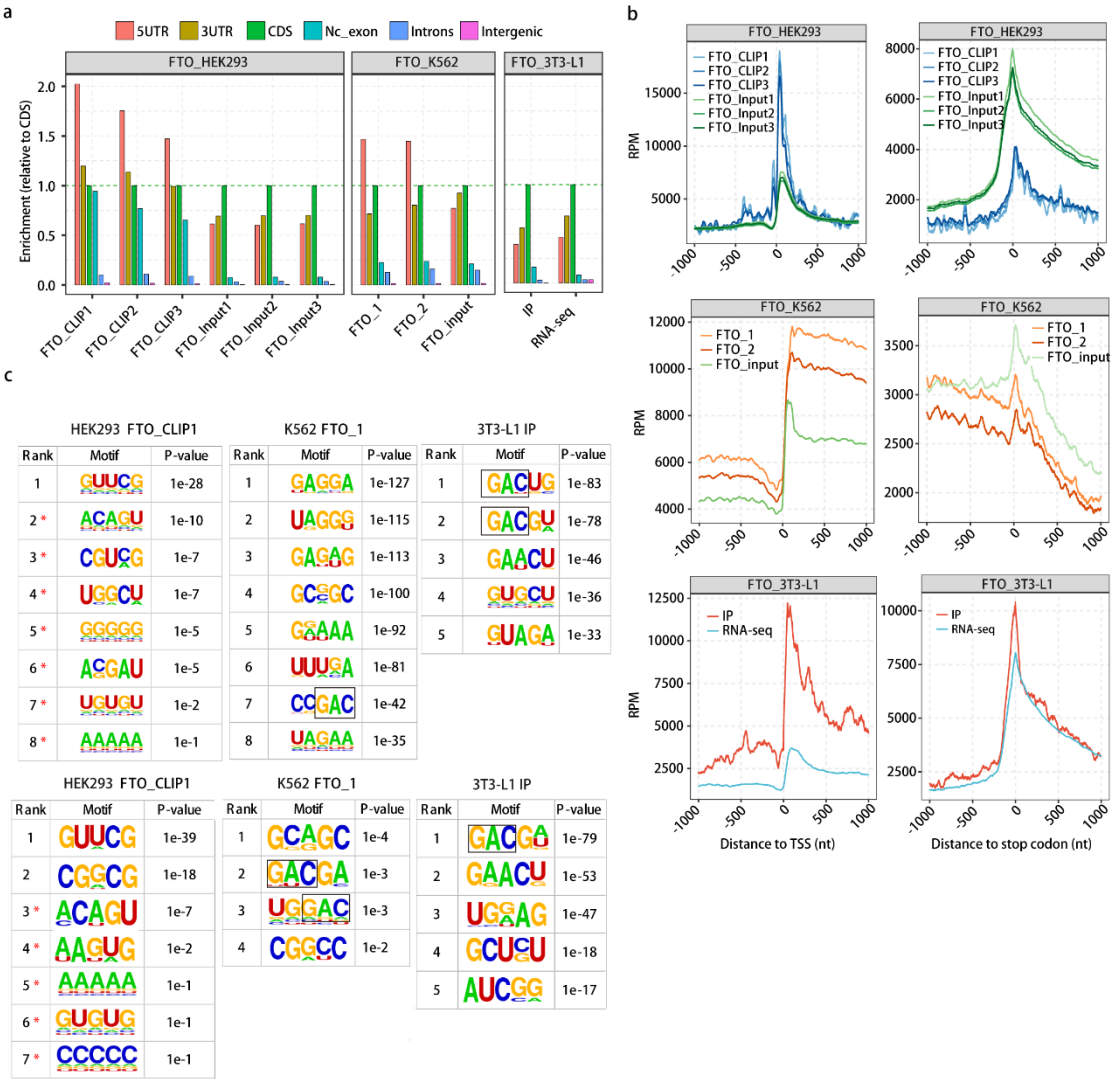

Fig. 1

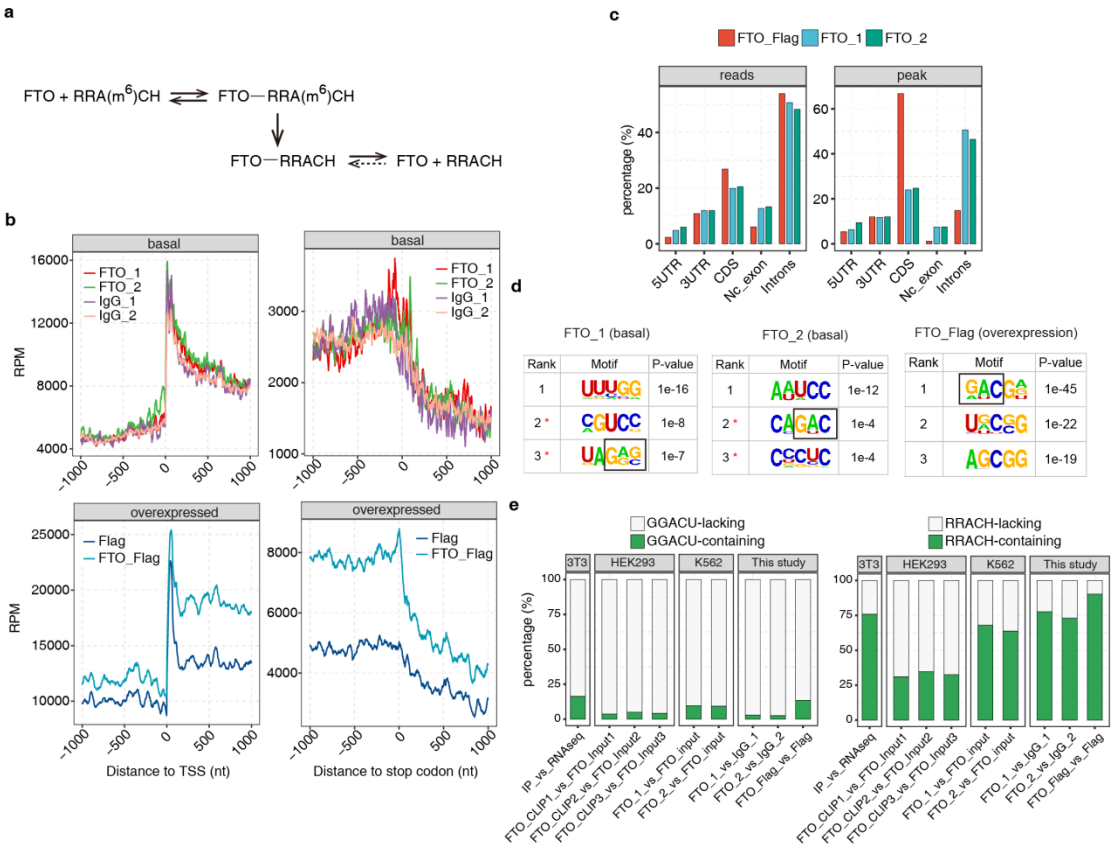
a
FTO + RRA(m6)CH
FTO—RRA(m6)CH
FTO—RRACH
FTO + RRACH
b
basal
FTO_1
FTO_2
IgG_1
IgG_2
RPM
overexpressed
Flag
FTO_Flag
Distance to TSS (nt)
Distance to stop codon (nt)
c
FTO_Flag
FTO_1
FTO_2
reads
peak
percentage (%)
5UTR
3UTR
CDS
Nc_exon
Introns
d
FTO_1 (basal)
FTO_2 (basal)
FTO_Flag (overexpression)
Rank
Motif
P-value
1e-16
1e-8
1e-7
1e-12
1e-4
1e-4
1e-45
1e-22
1e-19
e
GGACU-lacking
GGACU-containing
RRACH-lacking
RRACH-containing
3T3
HEK293
K562
This study
IP_vs_RNAseq
FTO_CLIP1_vs_FTO_Input1
FTO_CLIP2_vs_FTO_Input2
FTO_CLIP3_vs_FTO_Input3
FTO_1_vs_FTO_input
FTO_2_vs_FTO_input
FTO_1_vs_IgG_1
FTO_2_vs_IgG_2
FTO_Flag_vs_Flag

Fig. 2

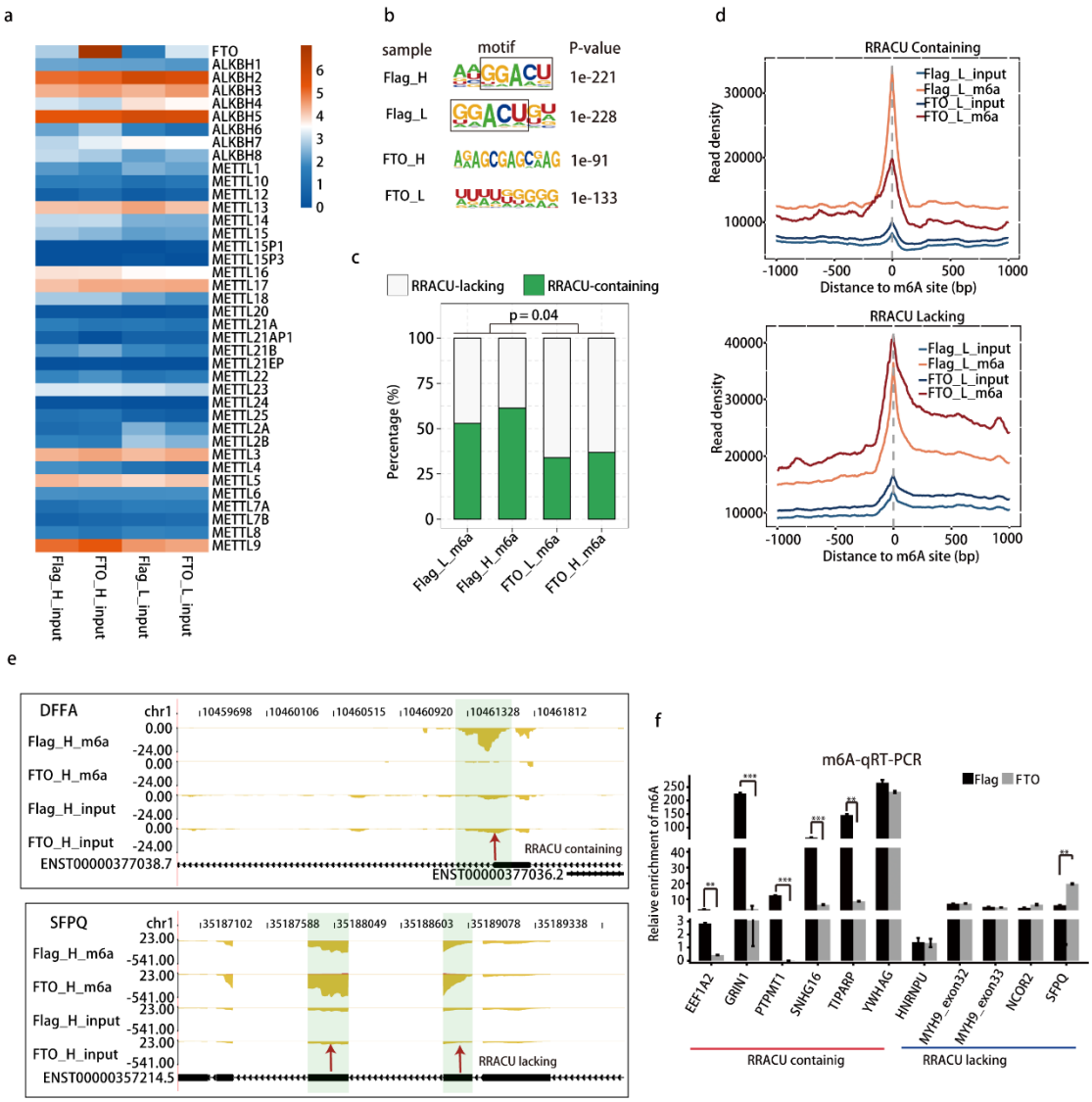
a
FTO
ALKBH1
ALKBH2
ALKBH3
ALKBH4
ALKBH5
ALKBH6
ALKBH7
ALKBH8
METTL1
METTL10
METTL12
METTL13
METTL14
METTL15
METTL15P1
METTL15P3
METTL16
METTL17
METTL18
METTL20
METTL21A
METTL21AP1
METTL21B
METTL21EP
METTL22
METTL23
METTL24
METTL25
METTL2A
METTL2B
METTL3
METTL4
METTL5
METTL6
METTL7A
METTL7B
METTL8
METTL9
6
5
4
3
2
1
0
Flag_H_input
FTO_H_input
Flag_L_input
FTO_L_input
b
sample
motif
P-value
Flag_H
1e-221
Flag_L
1e-228
FTO_H
1e-91
FTO_L
1e-133
c
RRACU-lacking
RRACU-containing
p = 0.04
Percentage (%)
100
75
50
25
0
Flag_L_m6a
Flag_H_m6a
FTO_L_m6a
FTO_H_m6a
d
RRACU Containing
Flag_L_input
Flag_L_m6a
FTO_L_input
FTO_L_m6a
Read density
30000
20000
10000
-1000
-500
0
500
1000
Distance to m6A site (bp)
RRACU Lacking
Flag_L_input
Flag_L_m6a
FTO_L_input
FTO_L_m6a
Read density
40000
30000
20000
10000
-1000
-500
0
500
1000
Distance to m6A site (bp)
e
DFFA
chr1
10459698
10460106
10460515
10460920
10461328
10461812
Flag_H_m6a
FTO_H_m6a
Flag_H_input
FTO_H_input
0.00
-24.00
RRACU containing
ENST00000377038.7
ENST00000377036.2
SFPQ
chr1
35187102
35187588
35188049
35188603
35189078
35189338
Flag_H_m6a
FTO_H_m6a
Flag_H_input
FTO_H_input
23.00
-541.00
RRACU lacking
ENST00000357214.5
f
m6A-qRT-PCR
Flag
FTO
Relaive enrichment of m6A
EEF1A2
GRIN1
PTPMT1
SNHG16
TIPARP
YWHAG
HNRNPU
MYH9_exon32
MYH9_exon33
NCOR2
SFPQ
RRACU containig
RRACU lacking

Fig. 3

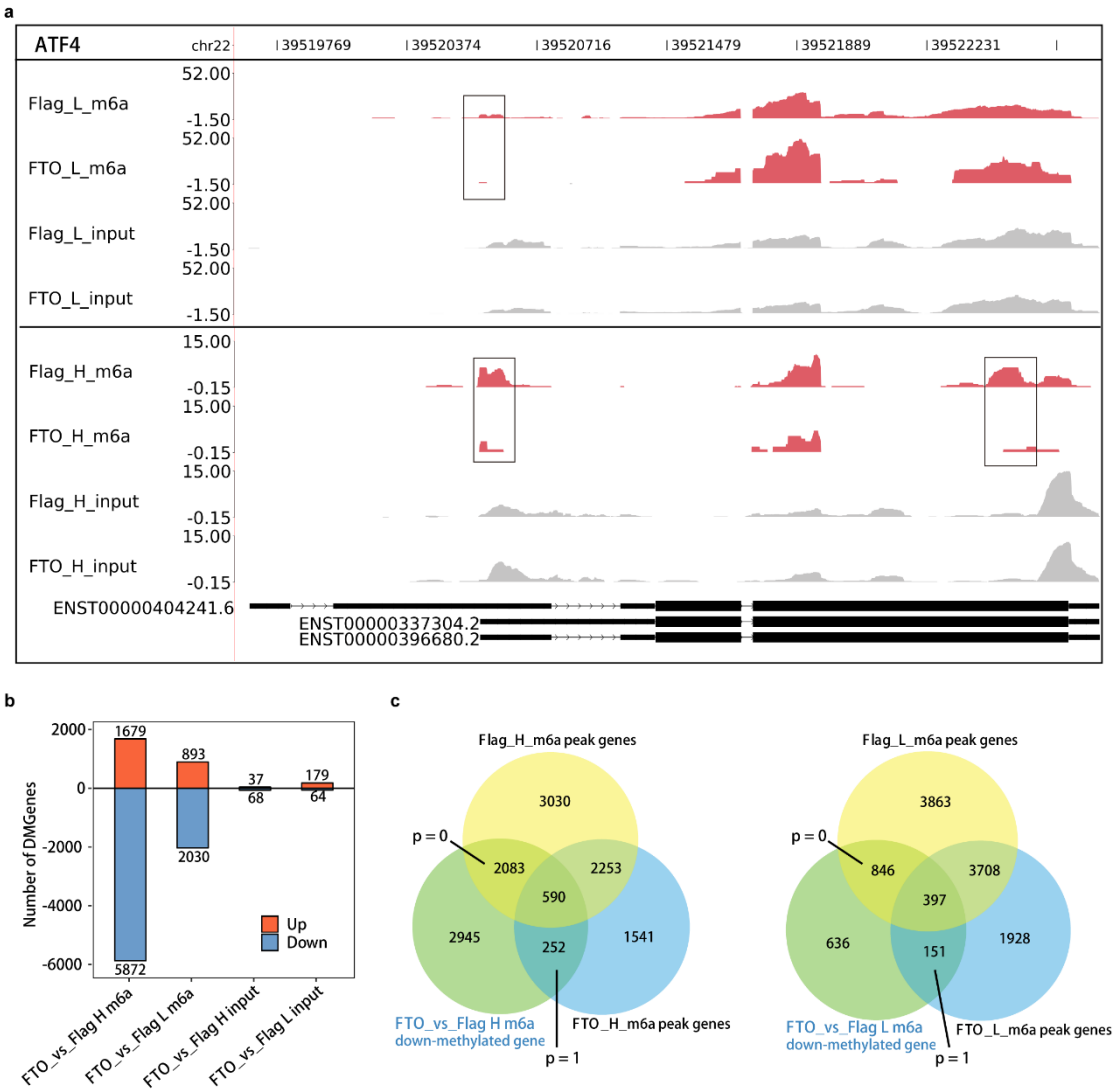
a
ATF4
chr22
39519769
39520374
39520716
39521479
39521889
39522231
Flag_L_m6a
FTO_L_m6a
Flag_L_input
FTO_L_input
Flag_H_m6a
FTO_H_m6a
Flag_H_input
FTO_H_input
ENST00000404241.6
ENST00000337304.2
ENST00000396680.2
b
Number of DMGenes
Up
Down
FTO_vs_Flag H m6a
FTO_vs_Flag L m6a
FTO_vs_Flag H input
FTO_vs_Flag L input
c
Flag_H_m6a peak genes
Flag_L_m6a peak genes
p = 0
p = 1
FTO_vs_Flag H m6a down-methylated gene
FTO_H_m6a peak genes
FTO_vs_Flag L m6a down-methylated gene
FTO_L_m6a peak genes

Fig. 4

Figure captions

Figure 1 Transcriptome-wide landscape of FTO binding shows cell type-specificity. Three recently published FTO eCLIP/CLIP-seq data were analyzed.

(**a**) FTO-binding reads were enriched in 5'UTR in HEK293 and K562, but not 3T3-L1 cells. CLIP/eCLIP reads mapped to each region of genome was normalized by the length of the region. There is no replicate and input control for 3T3-L1 cell, a suggested RNA-seq data was analyzed as input control. The enrichment of each region was calculated relative to CDS region. Nc_exon, non-coding exon.

(**b**) Enrichment of FTO binding around the transcription start site (TSS) and stop codons was different among HEK293, K562 and 3T3-L1 cells. Normalized FTO binding reads count (RPM) in a ± 1000 bp window around TSS (left) and stop codons (right) for all transcripts. RPM, reads per million.

(**c**) GAC-containing motifs were enriched in K562 and 3T3-L1, but not in HEK293 cells. The 5-nt FTO binding motifs were detected from ABLIRC peaks by HOMER. Those from one sample were presented, and all others were shown in Fig. S2. Motifs include GAC-consensus were marked with a black box. Original usable reads (upper) and randomly selected same number (102,470) of usable reads (lower) were used for peak calling and the motif analysis, respectively.

Figure 2 FTO selectively binds to m^{6}A motifs in HeLa cells, and the exogenously overexpressed FTO shows higher selectivity.

(**a**) A model shows the proposed dynamics of reactions forming FTO-RRACH and FTO-RRA(m^{6}A)CH that could be captured by anti-FTO immunoprecipitation.

(**b**) FTO CLIP reads were not enriched around the TSS or 5'UTR region compared to IgG control in normal HeLa cells (upper panel), but were enriched in all transcribed regions when captured the overexpressed Flag-FTO (lower panel). Normalized FTO binding reads count in a ± 1000 bp window around TSS (left) and stop codons (right) for CLIP-seq data. FTO_1 and FTO_2, and IgG_1 and IgG_2, represent two replicated CLIP-seq data obtained from normal HeLa cells using anti-FTO and anti-IgG antibodies, respectively. FTO_Flag represents CLIP-seq data obtained from HeLa cells transfected with plasmid expressing FTO-Flag fusion protein, and Flag represents that from the control HeLa cells transfected with Flag-only plasmid. RPM, reads per million.

(**c**) FTO binding were increased in the protein coding regions upon overexpression. Genomic distribution of FTO binding reads (left) and peaks (right) in HeLa cells.

(**d**) The top FTO binding motifs detected by HOMER.

(**e**) The fractions of FTO binding peaks containing GGACU and RRACH motifs were different among 3T3-L1, HEK293T, K562 and HeLa cells. The overexpressed FTO shows higher fractions of GGACU and RRACH-containing peaks in HeLa cells.

Figure 3 m^{6}A demethylation by FTO is RRACU-dependent in HeLa cells.

(**a**) FTO overexpression did not affect the expression of other m^{6}A writers and erasers in m^{6}A-seq input samples, which were polyadenylated RNAs. FTO-H and FTO-L represent samples from HeLa cells with high-fold (22.2) or low-fold (4.3) FTO overexpression in relative to the Flag-control, respectively. Normalized FPKM values of each gene was presented.

(**b**) GGACU motif was the top first motif in m^{6}A peaks from control HeLa cells, which was disappeared upon FTO overexpression.

(**c**) Relative proportions of m^{6}A peaks with or without RRACU motifs. RRACU-bearing m^{6}A peaks were detected in a higher frequency in Flag-control cells than that in FTO-Flag cells with FTO overexpression ($P < 0.05$). The *P* values were determined using Student's unpaired *t* test. FTO-H and FTO-L were regarded as replicates.

(**d**) Metagene distribution of m^{6}A-seq reads around the center of m^{6}A peaks identified in Flag-control cells. m^{6}A peaks were divided into two groups according to the presence or absence of the RRACU motif.

(**e**) Examples of FTO demethylation from mRNA transcripts at the m^{6}A peak containing a RRACU motif (DFFA), but not at the m^{6}A peak lacking a RRACU motif (SFPQ) in HeLa cells. The m^{6}A read density as shown for each gene in reads per million (RPM). Each gene was diagrammed by vertical black bars (exons) and thin horizontal lines (introns). m^{6}A peak regions were shadowed by light green rectangles and arrow.

(**f**) m^{6}A qRT-PCR validation of the RRACU-dependence in FTO demethylation of m^{6}A. The *P* values were determined using Student's unpaired t test. * $P < 0.05$. ** $P < 0.01$. *** $P < 0.001$. Results are shown as mean ± SE.

Figure 4 The extent of FTO demethylation is concentration-dependent.

(**a**) FTO-mediated demethylation of m^{6}A in gene ATF4 is concentration-dependence. FTO-demethylated regions were marked with black box.

(**b**) The number of genes whose mRNA/lncRNA methylation levels were down-regulated by FTO overexpression were 2.3-3.5 folds of the up-regulated, and increased with FTO levels. The number of up-regulated and down-regulated DMGs were showed in bar plot.

(**c**) FTO down-methylated genes are significantly overlapped with the m^{6}A peak genes in both high-fold and low-fold FTO overexpression samples. The *p* values indicated statistical significance of the number of overlapping genes.